Fuel 319 (2022) 123796

Contents lists available at ScienceDirect

Fuel

journal homepage: www.elsevier.com/locate/fuel

A comparative analysis and optimization of two supersonic hybrid SOFC and turbine-less jet engine propulsion system for UAV

Mehran Bahari [a,*], Majid Rostami [b], Ashkan Entezari [c], Sheida Ghahremani [d], Melika Etminan [b]

[a] School of New Technologies, Iran University of Science & Technology, Iran
[b] Department of Mechanical Engineering, Science and Research Branch, Islamic Azad University, Iran
[c] Faculty of New Science and Technologies, University of Tehran, Iran
[d] Faculty of Geodesy and Geomatics Engineering, K. N. Toosi University of Technology, Iran

ARTICLE INFO

Keywords:
UAV
Supersonic
Multi-objective optimization
SOFC
Turbine-less jet engine

ABSTRACT

In this study, we compared two different types of propulsion systems for a supersonic unmanned aerial vehicle (UAV) flying at Mach 1.8, which are using two different types of fuel to determine their characteristics and advantages. Also, investigate the effect of various factors such as altitudes and key design parameters of the propulsion system on efficiency and flight duration. These proposed propulsion systems are using a solid oxide fuel cell (SOFC) to generate the heat required for the operation of the turbine and generate thrust. The hydrogen for SOFC is either stored in the tank or generated by the internal reformation of methane inside the fuel cell. We studied the effects of several key design parameters for these engines in different flight conditions and altitudes; carrying out a multi-objective optimization for each proposed propulsion system to maximize the thrust of the engine while keeping the fuel consumption at a minimum rate to achieve the longest flight duration. Then we determined the best conditions where the acceptable thrust is accompanied by reasonable flight duration. Results indicated that the efficiency and generated power of the propulsion system will increase by higher flight altitude or compressor pressure ratio. Also, due to the recirculation of fuel in the SOFC's anode, we observed higher efficiency in comparison when hydrogen is used; since anode-recirculation causes higher fuel utilization. The optimization result shows that the efficiency and fuel consumption for the hydrogen-fueled system is 48.7% and 0.0024 kg/s, respectively, and 67.9% and 0.0066 kg/s. for the methane-fueled engine.

1. Introduction

SOFCs, facilities with considerable capability of conserving energy have been investigated from different aspects as the experimental study cases and numerical simulation attempts. Stambouli et al. [1] has outlined the global population growth and the growing need for energy and its environmental impacts. Zhang et al. [2] has reviewed the different concepts and strategies for overcoming climate change and energy security challenges by using the SOFC integrated systems. Buonomano et al. [3] has reviewed the SOFC-GT integrated systems that use alternative fuels like coal and biomass. Bae et al. [4] has investigated a dynamic model of the SOFC under electrical load change. The results have shown that the overall behavior is mostly related to the diffusion in the anode. As an innovative power source for portable application in vehicles, the SOFCs was subjected to many analyses incorporated with many commercial projects. STALKER-XE as a SOFC-powered UAV was experimentally applied by the Advanced Research Projects Agency [5]. They concluded considerable endurance for UAVs with the SOFC power resource in comparison with battery-powered ones. Volvo [6] completed the process of production and testing diesel heavy-duty truck which uses SOFC as an auxiliary power unit (APU). Their results introduced SOFC APU as an important facility in the body of the power generation system in their truck.

Analyzing and designing different types of high altitude and long-endurance unmanned aerial vehicles (UAVs) which are capable of operating at different missions like surveying, inspections, etc. are mainly being subjected to many types of researches [7]. Over the past years, aviation technology scientists became interested in publicizing the operation of UAV propulsion systems. Cirigliano et al. [8] has compared the Diesel, Spark-ignition, and turboprop engines for long-endurance missions. Bahari et al. [9] has studied the combination of

* Corresponding author.
E-mail addresses: mehran_bahari@nt.iust.ac.ir (M. Bahari), rostamimajid9574@gmail.com (M. Rostami), ashkan.entezari@ut.ac.ir (A. Entezari), ghahremani-sh@alumni.kntu.ac.ir (S. Ghahremani), melika.etminan@srbiau.ac.ir (M. Etminan).

https://doi.org/10.1016/j.fuel.2022.123796
Received 7 January 2022; Accepted 5 March 2022
Available online 12 March 2022

Nomenclature

A_c	area of the cell (m^2)
C_p	Specific heat capacity (kj/kmol.K)
D_{eff}	Gaseous diffusivity (m^2/s)
E_{act}	activation energy (kJ/mol)
F	constant of Faraday (C/g.mol)
F_s	Specific thrust (N/(kg/s))
G	free energy of Gibbs
k_e	pre-exponential factor
h	Specific enthalpy (kj/kg)
H	Enthalpy (kj)
j_0	Exchange current density (A/m^2)
j	Current density (A/m^2)
L	Fuel cell length (m)
m	Mass (kg)
$\dot{m}$	Mass flow (kg/s)
$\dot{n}$	molar mass flow rate (kmol/s)
n_e	Electrons transferred per action
N_c	number of cells
P	Pressure (bar)
P_{cell}	Power (kw)
q	The rate of heat (kj/s)
Q_r	Low heat value of fuel (kj/kg)
r_k	Reaction rate
R_{ohmi}	Fuel cell internal resistance (Ω)
S	Entropy (kj/kg.K)
$\overline{R}$	Universal gas constant
R	compressor pressure ratio
R_0	resistance (Ω)
π	Pressure ratio
T	Temperature (K)
V	Fuel cell voltage (V)
u	Flight velocity (m/s)
W	Fuel cell width (m)
U_f	Consumption of fuel
η	Efficiency
ξ	Coefficient of pressure recovery
γ	Specific heat ratio
τ	Thickness (m)
σ	Electronic conductivity

Subscript

a	Air
acti	Activation polarization
anode	anode
blow	blower
Comb	combustor
Comp	Compressor
conc	Concentration polarization
c	Fuel cell
Cath	Cathode
e	exit, output
Ex	Heat exchanger
Elec	Electrochemical reaction
Fa	Fuel inside reformer
Fb	Fuel inside combustor
F	Fuel
FC	fuel cell (as a stack)
Inta	Intake
i	Inlet
Nozz	Nozzle
ohmi	Ohmic polarization
Out	Outlet
Over	Overall
Prop	propulsion
R	reforming reaction
S	shifting reaction
Ther	thermodynamic
TPB	Three-phase boundaries

the fuel cell and internal combustion engine in a UAV. Gas turbine hybrid engines that utilize SOFCs have such a good propulsion capacity that can help electric UAVs to attain long endurance and high efficiency [10]. The turbine-less hybrid propulsion system which contains a solid oxide fuel cell (SOFC) is known as high effective performance equipment in the body of UAVs [11].

In the past several years, many attempts have been conducted to numerous pieces of research about the capability of combining SOFCs and gas turbines. Tucker [12] has tried to develop and optimize the high power density metal-supported SOFC. Giacoppo et al. [13] have investigated the thermal challenges in dissipation of the fuel cell's generated heat inside the UAV fuselage. Azizi et al [14] have represented a review on designing, controlling, analyzing, and optimization of the SOFC-GT systems. The hybrid systems which include SOFCs and gas turbines can be applied in aircraft as propulsion and electric generation sources. In this regard, Aguiar et al. [15] has investigated the high altitude and long endurance UAVs. They find that using multiple stack design can improve efficiency. Waters et al. [16] have investigated the engine-integrated catalytic partial oxidation reactors with SOFC. They reported an increase in fuel efficiency for their setup. Himansu et al. [17] concluded that the hydrogen-fueled gas turbine hybrid propulsion systems coupled with SOFCs can have much higher efficiency in comparison to internal combustion engines so that the hybrid one can be applied for HALE UAVs for long-duration missions between 10 and 20 days. According to Aguire et al. [15], the efficiency of the SOFC gas turbine hybrid system can be evaluated up to 66.3% for the case of SOFC with three stacks in hybrid system configuration. Okai et al. [18–20] found out that a hybrid system can operate as the main power source for distributed propulsion aircraft due to their considerable efficiency of electric generation. Collins et al.[21] introduces a fuel cell gas turbine hybrid arrangement that uses liquid Hydrogen as fuel and superconductive motors. A setup that can achieve 20 times the energy storage of state-of-the-art batteries. Fernandes et al. [22] realized that due to a considerable decrease of entropy in process of hydrogen preheating, it cannot be a suitable fuel for aircraft. Besides Results showed that the SOFC-GT system provides remarkable higher exergy efficiency when compared to the other conventional competing propulsion systems. Pan et al. [23] provide a general review on fuel cell working principles categorizing the fuel cell in two pure fuel and hybrid types and provided design methods for a practical flight test. Yanovski et al. [24] showed that in SOFC/GT hybrid systems we can see high efficiency in the case of using liquefied natural gas or liquid hydrogen. Seyam et al. [25] studied five different fuels for their novel propulsion system and compared their operation performance through system efficiency. They reported the net power of the propulsion system and carbon emission in case of using different fuels or a combined fuel in specific percentages from those five fuels. Seyam et al. [26] also performed an exergetic assessment SOFC based propulsion system to potentially improve the aviation performance with energetic and exergetic approaches. After comparing different fuel blends, they concluded that energetic and exergetic efficiencies will remain almost the same regardless of the fuel they use. They concluded that the cost of the fuel plays a more major role compared to energetic and exergetic efficiencies in selecting a new fuel blend. Fundamental complementary investigations were included in

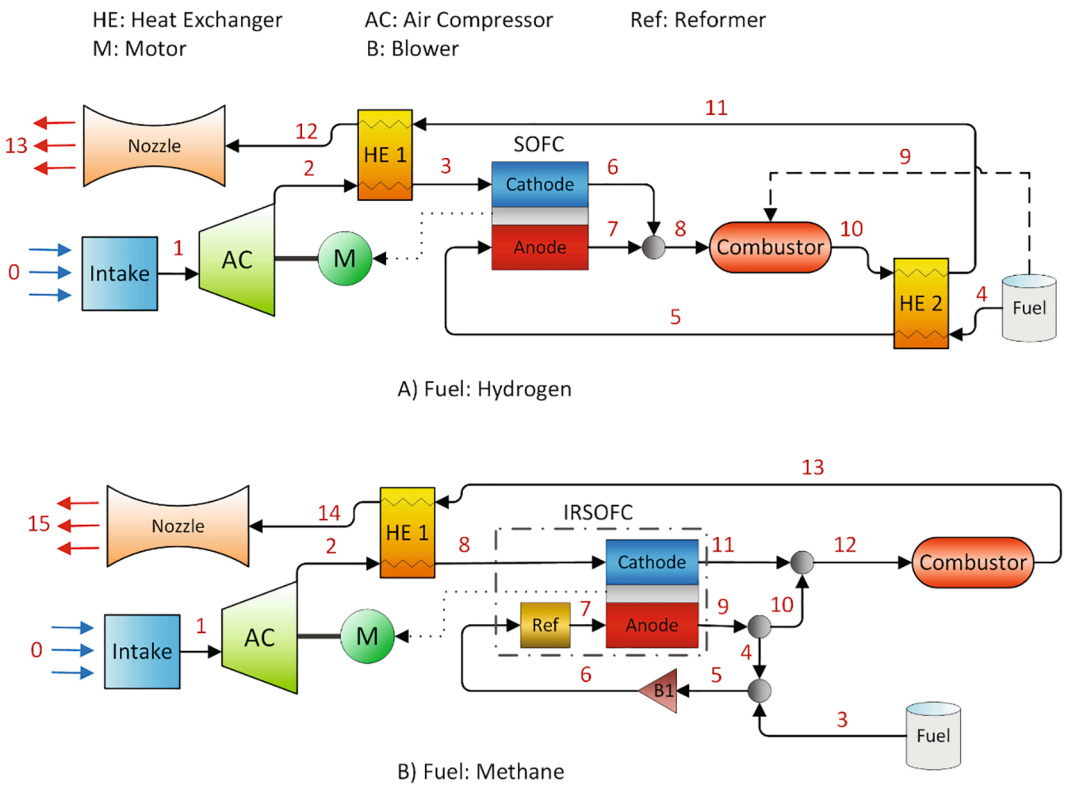

Fig. 1. Schematic diagram of the SOFC integrated turbine-less jet engine with different fuels.

many analyzes of SOFC-GT hybrid systems. Choudhury et al. [27] have reviewed the SOFC technology in power generation. Bao et al. [28] provides a comprehensive review in the state-of-the-art macroscopic SOFC model and SOFC integrated GT control-based models. Stiller [29] has presented a design, optimization and control method for the SOFC-GT hybrid system. Mahmoudi et al. [30] have thermodynamically and exergetically assessed the operation of the SOFC-GT system. Lv et al. [31] have provided a mathematical model for an intermediate temperature SOFC integrated system with a GT, fueled by gasified biomass. They have investigated the effects of the operation parameters on the system efficiency. They also have investigated the effects of the steam on the performance of the system [32]. In another paper, they also have investigated the effect of the gasified biomass on system load characteristics [33].

There is numerous paper that has investigated the areas of safe operation in SOFCs. In this regard, Zhixing Ji et al. [34] have studied the most recent safe zone operation of a hybris SOFC combined with an electric jet engine. They reported that turbine inlet temperature has no restricting effect on the engine. Also, in the case of low air and fuel flow rates, zones with too low reforming temperature and open-circuit voltage for SOFC exist. They also reported an unbalance energy zone and lower boundary of the safe zone. Lv et al. [33] have also investigated the safety performance of the SOFC-GT hybrid system fueled by the gasified biomass. They have also proposed a novel approach to determine the safe zone in the SOFC-GT hybrid systems [35].

Entirely, not so many investigations can be found about generating propulsive power by gas turbine hybrid systems that contain SOFC [9]. corresponding to Jansen et al. [36], the main factors of the aircraft propulsion system are specific power and efficiency. Bryce et al. [37] confirmed that propulsion systems of hybrid gas turbines that contain a fuel cell owe rarely low energy and power necessities, which are approximately not affected by the volume and weight of the propulsion system. UAVs that are suitable for high altitude and long-endurance (HALE) missions, light aircraft, etc. are kinds of equipment that are proper for these applications.

Ly et al. [38] offered the idea of turbine-less jet engines due to the difficult adjustment of the combustion chamber outlet temperature which was the result of turbine blade materials' thermal properties. They proposed their analysis toward simulation and experiment of turbine-less jet engine operation. Buchanan et al [39,40] applied the computational fluid dynamics method besides experimental tests to approach results that include higher efficiency and operation cost reduction of turbine-less jet engines in comparison with jet engines. Zhixing Ji et al. [41] have performed a performance and size optimization on the turbine-less integrated SOFC. They studied how the weight of the fuel cell affects fuel consumption. They concluded that there is a strong relationship between size and flight endurance. They reported that flight endurance first increases then decreases compared to turbojet engines as the fuel cell size and weight increases.

The capacity of solid oxide fuel cells (SOFCs) in working at high temperatures makes them beneficial in coupling with gas turbines. accordingly, they can be best-fitted pieces of equipment for operating beside turbine-less jet engines.

Regardless of innovation in the thermodynamics cycle structure of turbine-less jet engines, there are some obstacles that are the output of battery-powered compressors that can decrease the total efficiency of the system. Because of the large volume size of the battery, we see a low power-weight ratio in comparison to them with fuels. Being overweighted for turbine-less jet engines is the consequence of increasing battery power, thus utilizing these kinds of engines for long endurance operations cannot be done. furthermore, a fixed amount of battery-powered UAVs weight during the commission concludes the decrease in efficiency which is the main challenge of supplying electric power for their compressors in the case of being turbine less.

By comparing the specific power of conventional turbojet engines with turbine-less jet engines, the superiority of turbine-less ones was concluded which was due to the higher efficiency of the SOFC in generating the electricity and the replacement of the compressor with an electric motor. SOFCs have the capacity of generating a remarkable amount of electric power for consumption in the motor. In addition, the

outlet temperature of SOFCs can be high enough to be used by a turbine-less jet engine [38,40]. Ji et al. [42,43] have been thermodynamically investigated a turbine-less jet engine performance. They have improved the specific thrust and impulse of the engine.

Operation conditions of a high-speed UAV especially in supersonic conditions which are equipped with a SOFC-GT hybrid system is a challenging task that was not investigated as much as thermal efficiency and fuel consumption in the previous publications of aviation industry researchers Although there are many kinds of research investigating the operational characteristics, strong points, and drawbacks of the combined propulsion system of SOFC and turbine-less jet engines. Previous studies have more focused on the subsonic propulsion systems. There is very little investigation regarding UAVs that flight in supersonic conditions. We have tried to cover this gap in this research field and investigate the possibility and characteristics of SOFC integrated turbine-less jet engine supersonic propulsion systems.

In this paper, we try to compare two different types of propulsion systems for a UAV flying at Mach 1.8, which are using two different types of fuel. And investigate the effect of various factors such as altitudes and key design parameters of the propulsion system on efficiency and flight duration.

2. System description

Fig. 1 indicates the schematic diagram of SOFC turbine-less jet engines, with hydrogen and methane as fuels. The SOFC jet engine can operate preferably in comparison to the turbojet engine due to higher specific thrust and thermal efficiency which is due to the higher temperature of the exhaust gasses from the engine compare to turbojet engines. Here is how the thermodynamic cycle generally operates. Initially, the intake and compressor boost the air pressure and temperature in the first and second stages of the process. Thereafter, hydrogen and hot air are supplied for the anode and cathode of SOFC. then, the outlet streams from the SOFC mixes with extra fuel in the combustor to be burnt the unused fuel in the SOFC and also adjust the inlet temperature of the nozzle. In the end, hot air after heating the inlet air of SOFC enters the nozzle to be expanded and generates propulsion power for the UAV. The difference of the two cycles with different fuels is compared with each other in Fig. 1. Fig. 1(a) indicates the diagram of the hydrogen-fueled SOFC jet engine. In the hydrogen-fueled system, two heat exchangers are used due to the considerably low temperature of liquid hydrogen and the limitation of the pinch point of the heat exchangers. Fig. 1(b) indicates the diagram of the methane-fueled SOFC jet engine. The high-pressure air is divided and applied in the reformer and cathode. There exists steam in the exhaust of the anode outlet which can be utilized by the reformer.

Two conventional fuels, the cryogenic liquid hydrogen, and cryogenic liquid methane were analyzed in proposed cycles. Using hydrogen and methane as the fuel of the SOFCs has some drawbacks like low volume energy density and difficult conditions of preparing low temperatures to liquefy them. However, the numerous investigations in the development of technology can provide the capability of applying hydrogen and methane as the fuel for power units in different kinds of vehicles like UAVs.

3. Mathematical model

3.1. Analysis assumption of simulation

To simplify the process of simulating the proposed propulsion system, several assumptions have been made for simplification, which is listed as follows:

1) The power unit system performance is considered a steady-state.
2) All power unit elements are adiabatic.
3) The air is composed of 21% oxygen and 79% nitrogen.
4) The operational temperature of fluids in the cathode and anode is the same.
5) The operating gaseous fluids are assumed to behave as the ideal gases.

3.2. Reformer model

The reformation of the methane fuel for the SOFC is a steam-reforming process that happens internally inside the SOFC. The recirculation of the Anode gasses provides the steam for the reformation process. The internal reforming process consists of two subprocesses. These two subprocesses are known as steam reforming and shifting processes. These processes and the overall electrochemical reaction inside the SOFC are as follow:

$$xCH_4 + xH_2O \rightarrow xCO + 3xH_2 \tag{1}$$

$$yCO + yH_2O \rightarrow yCO_2 + yH_2 \tag{2}$$

$$zH_2 + 0.5zO_2 \rightarrow zH_2O \tag{3}$$

Where x, y, and z are the numbers of moles.

These two processes are both equilibrium reactions; which means not all of the methane and carbon monoxide is converted to the righthand side of the equation. The exact amount which converts is related to factors such as temperature and pressure. The equilibrium constants for steam reforming (K_R) and shifting reaction (K_S) are as follow [9]:

$$K_R = \frac{\left(\frac{\dot{n}_{CO,i}+x-y}{\dot{n}_{tot,i}+2x}\right) \times \left(\frac{\dot{n}_{H_2,i}+3x+y-z}{\dot{n}_{tot,i}+2x}\right)}{\left(\frac{\dot{n}_{H_2O,i}-x-y+z}{\dot{n}_{tot,i}+2x}\right) \times \left(\frac{\dot{n}_{CH_4,i}-x}{\dot{n}_{tot,i}+2x}\right)} \times \left(\frac{P_{cell}}{P_{ref}}\right)^2 \tag{4}$$

$$K_S = \frac{\left(\frac{\dot{n}_{CO2,i}+y}{\dot{n}_{tot,i}+2x}\right) \times \left(\frac{\dot{n}_{H_2,i}+3x+y-z}{\dot{n}_{tot,i}+2x}\right)}{\left(\frac{\dot{n}_{CO,i}+x-y}{\dot{n}_{tot,i}+2x}\right) \times \left(\frac{\dot{n}_{H_2O,i}-x-y+z}{\dot{n}_{tot,i}+2x}\right)} \tag{5}$$

Where *i* and *ref* stand for inlet and reference conditions. And $\dot{n}$ is the molar mass flow rate.

By calculating the steam reforming and shifting reaction equilibrium constants from the Gibbs free energy and considering the fuel utilization inside the SOFC, from the above equations, the molar fraction (x, y and z) can be calculated [9].

$$\ln K_R = -\frac{\Delta \overline{g}_R^0}{\overline{R} \times T_{FC,e}} \tag{6}$$

$$\ln K_S = -\frac{\Delta \overline{g}_S^0}{\overline{R} \times T_{FC,e}} \tag{7}$$

$$U_f = \frac{z}{3x+y}$$

where

$$\Delta \overline{g}_R^0 = \overline{g}_{CO}^0 + 3\overline{g}_{H_2}^0 - \overline{g}_{CH_4}^0 - \overline{g}_{H_2O}^0 \tag{8}$$

$$\Delta \overline{g}_S^0 = \overline{g}_{CO_2}^0 + \overline{g}_{H_2}^0 - \overline{g}_{CO}^0 - \overline{g}_{H_2O}^0 \tag{9}$$

Also, $\overline{R}$ and $T_{FC,e}$ are universal gas constants (8.314 J/mol.K) and temperature at the Fuel cell outlet.

The steam reforming and shifting processes that are happening inside the SOFC to reform the methane to hydrogen requires a considerable amount of water (steam). Since we don't have an auxiliary unit to supply steam for these processes, a high recirculation ratio is needed to re-

Table 1
The partial pressure of H_2 and O_2 at the boundary of three-phase [9].

Equation	No.
$P_{H_2,TBP} = P_{H_2,f} - \frac{RT_{cell}\tau_{anode}}{2FD_{eff,anode}} j$	10
$P_{H_2O,TBP} = P_{H_2,f} + \frac{RT_{cell}\tau_{anode}}{2FD_{eff,anode}} j$	11
$P_{O_2,TBP} = p - \left(p - p_{O_2,a}\right)\exp\left(\frac{RT_{cell}\tau_{anode}}{4FD_{eff,anode}P} j\right)$	12

Table 2
the voltage and current density of the fuel cell [9].

Description	Equation	No.
Generated work	$\dot{W}_{FC} = V_c.j.A_c.N_c$	13
Current density	$j = \frac{2z.F}{N_c.A_c}$	14
Cell voltage	$V_c = V_{ner} - (V_{ohm} + V_{act} + V_{con})$	15
Nernst voltage	$V_{ner} = -\frac{\Delta G^0}{n_e F} - \frac{\overline{R}T_{FC}}{2F}\ln\left(\frac{P_{H_2O}}{P_{H_2}.(P_{O_2})^{0.5}}\right)$	16
Ohmic voltage loss	$V_{ohm} = (R_c + \sum_i \sigma_i t_i).j$	17
Electrolyte's ohmic resistance	$\sigma_{electrolyte} = (3.34 \times 10^4) \times \exp(-10300/T_{FC})$	18
Anode's ohmic resistance	$\sigma_{anode} = (9.5 \times 10^7) \times \exp(-1150/T_{FC})$	19
Cathode's ohmic resistance	$\sigma_{cathode} = (9.5 \times 10^7) \times \exp(-1200/T_{FC})$	20
Activation voltage loss	$V_{act} = V_{act,anode} + V_{act,Cathode}$	21
Anode's activation voltage loss	$V_{act,anode} = \frac{\overline{R}.T_{FC,e}}{F}\left(\sinh^{-1}\frac{j}{2j_{0,anode}}\right)$	22
Cathode's activation voltage loss	$V_{act,cathode} = \frac{\overline{R}.T_{FC,e}}{F}\left(\sinh^{-1}\frac{j}{2j_{0,cathode}}\right)$	23
Anode's exchange current density	$j_{0,anode} = \frac{\overline{R}.T_{FC,e}}{2F} k_{e,anode}\exp\left(-\frac{E_{act,anode}}{\overline{R}.T_{FC,e}}\right)$	24
Cathode's exchange current density	$j_{0,Cathode} = \frac{\overline{R}.T_{FC,e}}{2F} k_{e,cathode}\exp\left(-\frac{E_{act,cathode}}{\overline{R}.T_{FC,e}}\right)$	25
Concentration voltage loss	$V_{conc} = V_{conc,anode} + V_{conc,Cathode}$	26
Anode's concentration voltage loss	$V_{conc,anode} = \frac{\overline{R}.T_{FC,e}}{2F}\left(\frac{P_{H_2O}.P_{H_2,fuel}}{P_{H_2}.P_{H_2O,fuel}}\right)$	27
Cathode's concentration voltage loss	$V_{conc,cathode} = \frac{\overline{R}.T_{FC,e}}{4F}\left(\frac{P_{O_2,fuel}}{P_{O_2}}\right)$	28

Table 3
SOFC operational condition and contents [9].

Parameter	Value
Fuel utilization	0.8
Cell active area	0.01 m^2
Anode's exchange current density	6500 A/m^2
Cathode's exchange current density	2500 A/m^2
Anode's gaseous diffusivity	0.2×10^{-4} m^2/s
Cathode's gaseous diffusivity	0.05×10^{-4} m^2/s
Anode's thickness	0.05×10^{-2} m
Cathode's thickness	0.005×10^{-2} m
Electrolyte's thickness	0.001×10^{-2} m
Interconnector's thickness	0.3×10^{-2} m
Blower's Isentropic efficiency	0.85

Table 4
Equations for SOFC mathematical model.

Description	Equation	No.
The electrochemical reaction heat	$Q_{elec} = zT_{Cell}.\Delta S - j.(V_{ohmi} + V_{conc} + V_{acti,anode} + V_{acti,cathode}$	29
Steam reforming transformation reaction heat	$CH_4 + H_2O \leftrightarrow CO + 3H_2 Q_R$	30
Shifting reaction heat	$CO + H_2O \leftrightarrow CO_2 + H_2 Q_S$	31
Net generated heat in the fuel cell	$\dot{Q}_{net} = \dot{Q}_R + \dot{Q}_S + \dot{Q}_{elec}$	32

supply the produced steam at the outlet of the SOFC to its intake. For further information about the anode recirculation ratio, steam to carbon ratio, safety, and carbon decomposition refer to our previous paper [9].

3.3. SOFC model

A SOFC model for thermodynamic analysis is proposed in references [44,45]. According to the proposed propulsion systems, two different types of fuel can be used in the SOFC. Since the methane-fuel needs to reform the methane to hydrogen in order to be used in the fuel cell, many additional equations should be solved to simulate the process of converting methane to hydrogen. Besides, in this system, the anode recirculation loop maximizes the fuel utilization inside the SOFC which further adds to the complexity of the system.

The reaction of electrochemistry in the stack takes place at the three-phase boundary of the electrode [46] and the operational pressure of the flowing fluids can be obtained by equations which are represented in Table 1 [9].

The voltage and current density of the fuel cell can be obtained from the equations listed in Table 2.

The other constants used in the fuel cell modeling are listed in

Table 5
Thermodynamics Equations of the components.

Components	Equation	No.
Intake	$T_{out} = T_{in}\{1 + [\frac{\gamma-1}{2}]M_\infty^2$	33
	$P_{out} = P_{in}\left\{1 + \eta_{inta}\left[\left(\frac{T_{out}}{T_{in}}\right) - 1\right]\right\}^{\gamma/(\gamma-1)}$	34
	$\eta_{inta} = 1 - 0.075(M_\infty - 1)^{1.35}$	35
Compressor	$T_{out} = \left\{1 + \left(\frac{1}{\eta_{comp}}\right)\left[(\pi)^{\frac{\gamma-1}{\gamma}} - 1\right]\right\}T_{in}$	36
	$P_{out} = P_{in}\pi_{comp}$	37
	$W_{comp} = \dot{m}_{comp}(h_{comp,out} - h_{comp,in})$	38
	$\eta_{comp} = 0.91 - \frac{\pi_{comp} - 1}{300}$	39
Nozzle	$u_e = \sqrt{2\eta_{nozz} c_p T_{in}[1 - [\frac{p_a}{p_{in}}]^{(\gamma-1)/\gamma}]}$	40
	$p_{out} = p_a$	41
Combustor	$H_{comb,out} = H_{SOFC,out} H_{fb,in}$	42

Table 6
Efficiency coefficients of combustor and nozzle [47,51].

Component	Symbol	Value
Efficiency of combustor	η_{comb}	0.98
Multiplier of Combustor total pressure recovery	ξ_{comb}	0.99
Efficiency of nozzle	η_{nozz}	0.9

Table 7
working factors of the blower and heat exchanger [47,51].

Element	Symbol	Value
Efficiency of heat exchanger	η_{ex}	0.98
Gas section parameter of pressure recovery	$\eta_{ex,g}$	0.99
Adiabatic efficiency of the blower	η_{blow}	0.7
Blower pressure ratio	π_{blow}	1.1
Air section parameter of pressure recovery	$\eta_{ex,a}$	0.98

Table 8
Efficiency equations of the system.

Component	Unit	Equations	No.
Thermal efficiency	%	$\eta_{ther} = (KE_{gain})/(\dot{m}_f \times Q_r) \times 100$	46
Propulsion efficiency	%	$\eta_{prop} = \frac{2}{1 + u_e/u} \times 100$	47
Overall efficiency	%	$\eta_{over} = \eta_{ther}\eta_{prop} \times 100$	48

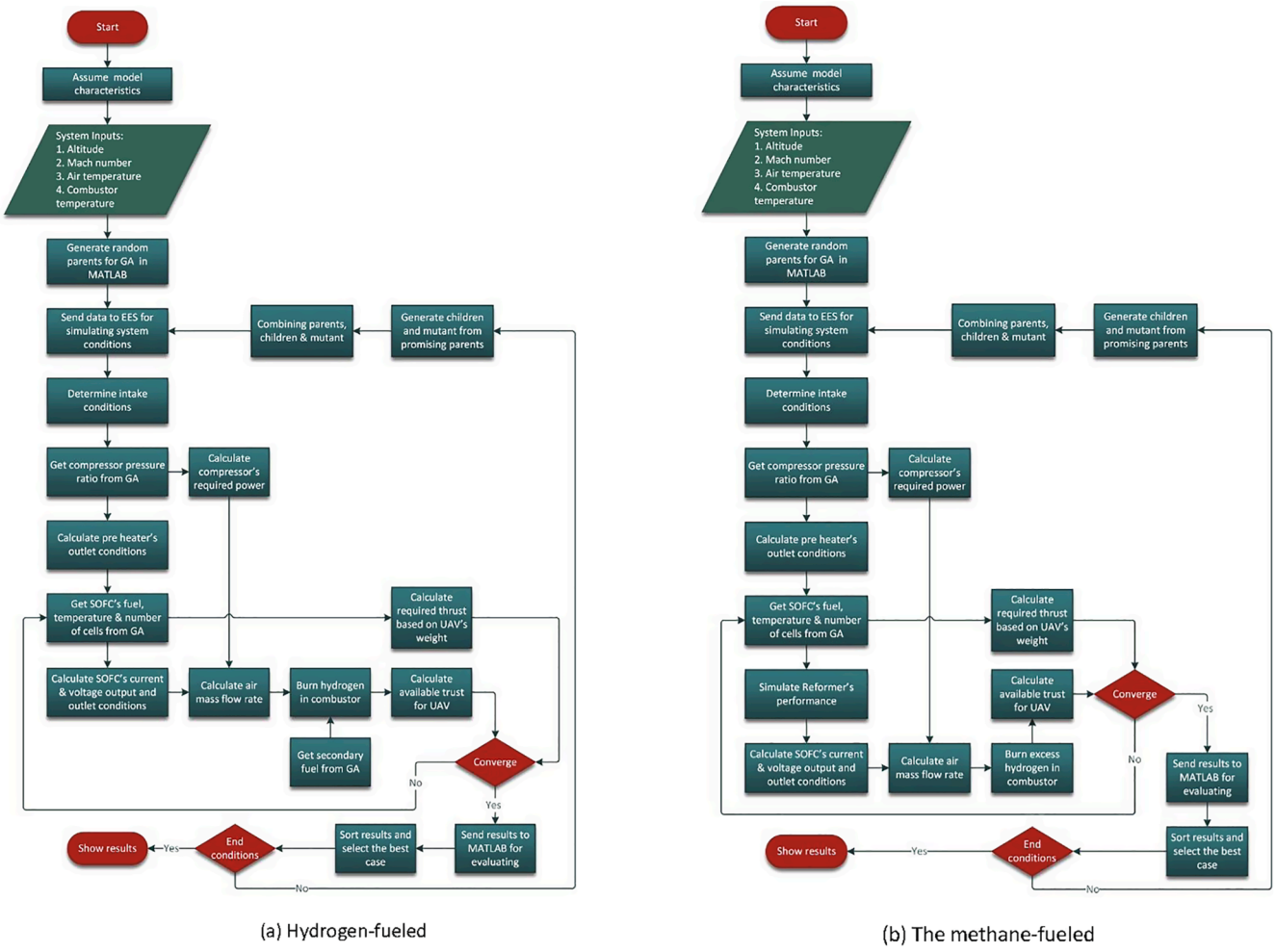

Fig. 2. Flowchart to investigate the performance of the suggested propulsion system.

Table 9
List of parameters for system optimization [9].

Key design and optimization parameters	Range or value
SOFC fuel mass flow rate (kg/s)	$0.001 < \dot{m}_{fuel} < 0.015$
Secondary fuel mass flow rate (kg/s)	$0 < \dot{m}_{fuel,2} < 0.0005$
Compressor pressure ratio	$5 < R < 25$
Anode recirculation ratio (for methane-fuel only)	$0.4 < alpha < 0.8$
SOFC's temperature (K)	$900 < T_{stack} < 1300$
SOFC's cell number	$1500 < N_C < 6000$
Papulation size	20
Max number of generations	250
Probability of off-spring	0.8
Probability of mutation	0.3
Mutation rate	0.02
Exploration	0.05
Number of crossover points	1
Selection Method	Roulette wheel
Selection pressure	5

Table 10
Simulated temperature and pressure for each point in the hydrogen-fueled system and data reported by Zhixing et al [51].

	This study		Zhixing et al.		Error	
Stage	T(K)	P(Bar)	T(k)	P(Bar)	T(K)	P(bar)
1	288	1.0	288	1	0.00	0.00
2	673.1	15.0	675	15	0.28	0.03
3	873	15.0	843	15	0.00	0.03
4	300	15.0	300	15	0.00	0.03
5	873	15.0	873	15	0.00	0.03
6	1016	14.3	1046	14	2.87	1.82
7	1016	14.3	1046	14	2.87	1.82
8	1016	14.3	1046	14	2.87	1.82
10	1147	14.3	1167	14	1.71	1.82
11	1053	14.3	993	14	6.04	1.82
12	923	14.3	946	14	2.41	1.82
13	490	14.3	516	1	4.98	1.82

Table 3. Also, the temperature gradient across the SOFC stack is considered to be less than 100 K.

The heat generated inside the fuel cell can be calculated based on the generated heat of the subprocesses inside the fuel cell which are shown in Table 4.

3.4. Jet engine model

The thermodynamic analysis equations of the intake, compressor, nozzle, and combustor in both suggested cycles are considered in Table 5.

The total pressure recovery coefficient of the intake is considered under the experimental results assumptions of NASA. The compressor adiabatic efficiency is calculated employing Korakianitis and Wilson equations [48]. For the standard operating condition of jet engines, the efficiency and total pressure recovery multiplier of the combustor and adiabatic efficiency of the nozzle applied in both cycles are listed in Table 6.

Table 11
Simulated temperature and pressure for each point in the methane-fueled system and data reported by Zhixing et al [51].

	This study		Zhixing et al.		Error	
Stage	T(K)	P(Bar)	T(k)	P(Bar)	T(K)	P(bar)
1	288	1.0	288	1	0.00	0.00
2	673.1	15.0	675	15	0.28	0.01
3	300	14.3	300	15	0.00	4.99
4	958.9	14.3	1008	14	4.87	1.79
5	908.4	14.3	896	14	1.38	1.79
6	918.9	15.0	912	16	0.76	6.24
7	925	14.3	874	15	5.84	4.99
8	873	15.0	873	15	0.00	0.01
9	958.9	14.3	1008	14	4.87	1.79
10	958.9	14.3	1008	14	4.87	1.79
11	958.9	15.0	1008	14	4.87	7.15
12	958.9	14.6	1008	14	4.87	4.47
13	1033	14.6	1078	14	4.17	4.47
14	850.6	14.6	898	14	5.28	4.47
15	466.8	1	487	1	4.15	0.00

Table 12
Efficiency, Cell voltage and thrust for the proposed systems and data reported by Zhixing et al [51].

	Hydrogen			Methane		
	This study	Zhixing et al	Error (%)	This study	Zhixing et al	Error (%)
Efficiency (%)	63.2	61.5	2.76	65.28	67.7	3.57
Cell voltage (V)	0.869	0.845	2.84	0.865	0.845	2.37
Thrust (N)	948.1	1000	5.19	903.2	970	6.89

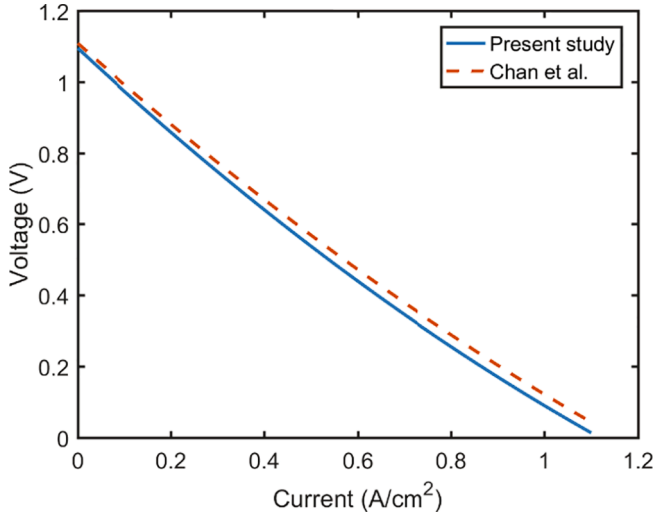

Fig. 3. Comparison of the voltage vs. current density of the present study's simulated model of SOFC and results reported by Chan et al. [46].

3.5. Heat exchanger and blower model

The analysis method of the heat exchanger generally depends on equations of energy conservation and the blower working temperature which is equal to the mixed gases temperature. The blower outlet condition can be calculated by the following equations:

$$T_{out} = \left\{1 + \left(\frac{1}{\eta_{blow}}\right)\left[\pi_{bow}{}^{\frac{\gamma-1}{\gamma}} - 1\right]\right\} T_{in} \tag{43}$$

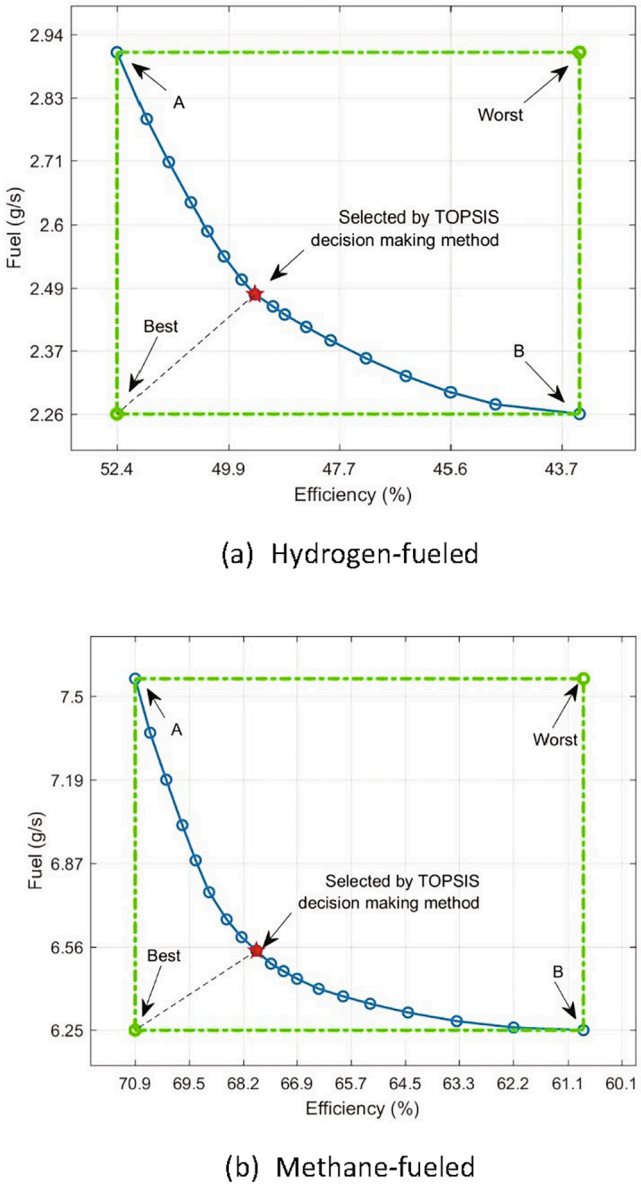

Fig. 4. The optimized points for fuel consumption and generated thrust of the two proposed systems.

Table 13
The optimized working conditions for the proposed propulsion systems.

Items	Hydrogen-fueled	Methane-fueled
Compressor pressure ratio	11.797	8.6502
SOFC's fuel mass flow rate (g/s)	2.3808	6.507
Combustor fuel mass flow rate (g/s)	0.0585	–
Anode recirculation ratio	–	0.8
Stack temperature	1064	1020.7693
SOFC's cell number	3332	5045.3183
Air (kg/s)	0.34032	0.593
Thrust (N)	182.8518	219.4525
Efficiency (%)	48.755	67.91
Fuel consumption(kg/s)	0.0024	0.0065

$$P_{out} = P_{in}\pi_{blow} \tag{44}$$

$$\dot{W}_{blow} = \dot{m}_{blow}\left(h_{blow,out} - h_{blow,in}\right) \tag{45}$$

The working condition of the heat exchanger and blower are shown in Table 7.

Table 14
Stream properties of the hydrogen-fueled propulsion system.

Stage	T (K)	P (Bar)	m (kg/s)	h (kj/kg)	H2O (%)	H2 (%)	N2 (%)	O2 (%)
0	223	0.26	0.3403	6465	0	0	79	21
1	367.9	1.38	0.3403	10,684	0	0	79	21
2	767.2	16.32	0.3403	22,778	0	0	79	21
3	954.9	16.32	0.3403	28,825	0	0	79	21
4	300	100.96	0.002381	8076	0	100	0	0
5	954.9	16.32	0.002381	27,284	0	100	0	0
6	1064	15.50	0.3262	30,946	0	0	82.08	17.92
7	1064	15.50	0.01655	63,467	75	25	0	0
8	1064	15.50	0.3427	34,010	7.066	2.355	74.35	16.23
9	300	100.96	0.0000585	8076	0	100	0	0
10	1205	15.50	0.3428	40,035	9.483	0.2611	75.05	15.21
11	1153	15.50	0.3428	38,208	9.483	0.2611	75.05	15.21
12	985.3	15.50	0.3428	32,464	9.483	0.2611	75.05	15.21
13	288.4	0.26	0.3428	8364	9.483	0.2611	75.05	15.21

Table 15
Stream properties of the methane-fueled propulsion system.

Stage	T (K)	P (Bar)	m (kg/s)	h (kj/kg)	CH4 (%)	CO2 (%)	CO (%)	H2O (%)	H2 (%)	N2 (%)	O2 (%)
0	223.3	0.26	0.5901	6472	0	0	0	0	0	79	21
1	368.3	1.41	0.5901	10,696	0	0	0	0	0	79	21
2	723.1	12.20	0.5901	21,391	0	0	0	0	0	79	21
3	300	11.59	0.006546	−117	100	0	0	0	0	0	0
4	1021	11.59	0.186	61,873	0.00316	18.65	1.055	72.92	4.861	1.985	0.5277
5	996.3	11.59	0.1926	59,765	4.699	17.78	1.006	69.49	4.633	1.892	0.5029
6	1008	12.20	0.1926	60,252	4.699	17.78	1.006	69.49	4.633	1.892	0.5029
7	1070	11.59	0.1941	56,196	0.00342	20.2	1.143	54.87	21.06	2.15	0.5715
8	995	11.59	0.5886	30,143	0	0	0	0	0	79	21
9	1021	11.59	0.2325	61,873	0.00316	18.65	1.055	72.92	4.861	1.985	0.5277
10	1021	11.59	0.0465	61,873	0.00316	18.65	1.055	72.92	4.861	1.985	0.5277
11	1021	11.59	0.5644	29,495	0	0	0	0	0	82.03	17.97
12	1021	11.59	0.6109	32,581	0.0003	1.778	0.1006	6.951	0.4634	74.4	16.3
13	1057	11.59	0.6109	34,055	6.03E-06	1.882	0.00202	7.426	0.00929	74.61	16.07
14	812.3	11.59	0.6109	25,810	6.03E-06	1.882	0.00202	7.426	0.00929	74.61	16.07
15	254.4	0.26	0.6109	7376	6.03E-06	1.882	0.00202	7.426	0.00929	74.61	16.07

3.6. Performance factors

For the suggested propulsion system in this study which SOFC has the main role in converting energy, Table 8 indicates several factors affecting the performances of fuel cells. The endurance can be estimated by specific impulse and the thrust-weight ratio is quantified by specific thrust. Moreover, propulsion efficiency and overall efficiency develop a relationship between the engine and the environment.

3.7. Solution method

The analysis of SOFC simulated operation begins with input data such as intake air temperature, compressor pressure ratio, fuel mass flow rate, flight Mach number and altitude, etc. The first step in simulating the proposed propulsion system is importing key design parameters from the Genetic algorithm in MATLAB which includes the compressor pressure ratio. Next based on intake air conditions, the properties of the outlet stream of the compressor can be calculated which will be used to simulate the voltage and current of SOFC based on the other imported key design parameters such as fuel mass flow rate, number of cells and stack temperature. Since the power generated by SOFC will operate the electric motor for the compressor, air mass flow rate can be calculated from the compressor pressure ratio and power generated by SOFC. Then unused fuel in SOFC will be burnt in the afterburner to generate the heat required for the generation of thrust in the nozzle. Additional fuel might be added if a higher thrust is needed based on the required thrust to weight ratio. Next, the results of the simulation will be sent to GA in MATLAB to sort the best answers and repeat the process to achieve the best solution which satisfies optimization goals. Fig. 2 demonstrates the overall procedures for simulation and optimization of the proposed system.

3.8. Optimization

Optimization algorithms are considered one of the promising methods for solving complex engineering problems when simple calculations are not effective in portrait the system reaction to the changes in operating conditions of system components [49]. Since in the proposed propulsion system, many of the key design parameters may conflict with each other, using heuristic numerical algorithms such as the Genetic algorithm (GA) can be extremely beneficial [50]. We defined two goals for optimization of the proposed propulsion system which are (1) maximizing the thrust and (2) minimizing the fuel consumption rate. These are the main goals of the aviation industry which can be interpreted as maximum efficiency. To design the proposed propulsion system to satisfy the goals we employed multi-objective optimization to maximize the thrust while minimizing the fuel consumption rate (i.e. maximizing the flight duration). For this purpose, we defined a new optimization target consisting of two separate dimensionless parameters as thrust and fuel consumption rate as shown in Eq. (49) By changing the weight (α) for each of these dimensionless parameters, a working curve will be generated that is known as the Pareto frontier. Finally, we used the TOPSIS decision-making method to select the best answer with an acceptable trade-off between Thrust and fuel consumption.

$$Obj. = \alpha \frac{Thrust_{max}}{Thrust} + (1-\alpha)\frac{Fuel\ \ mass\ \ flow\ \ rate}{Fuel\ \ mass\ \ flow\ \ rate_{min}} \tag{49}$$

Key design parameters and other constants that have been used in the optimization of the proposed system in this paper are listed in Table 9.

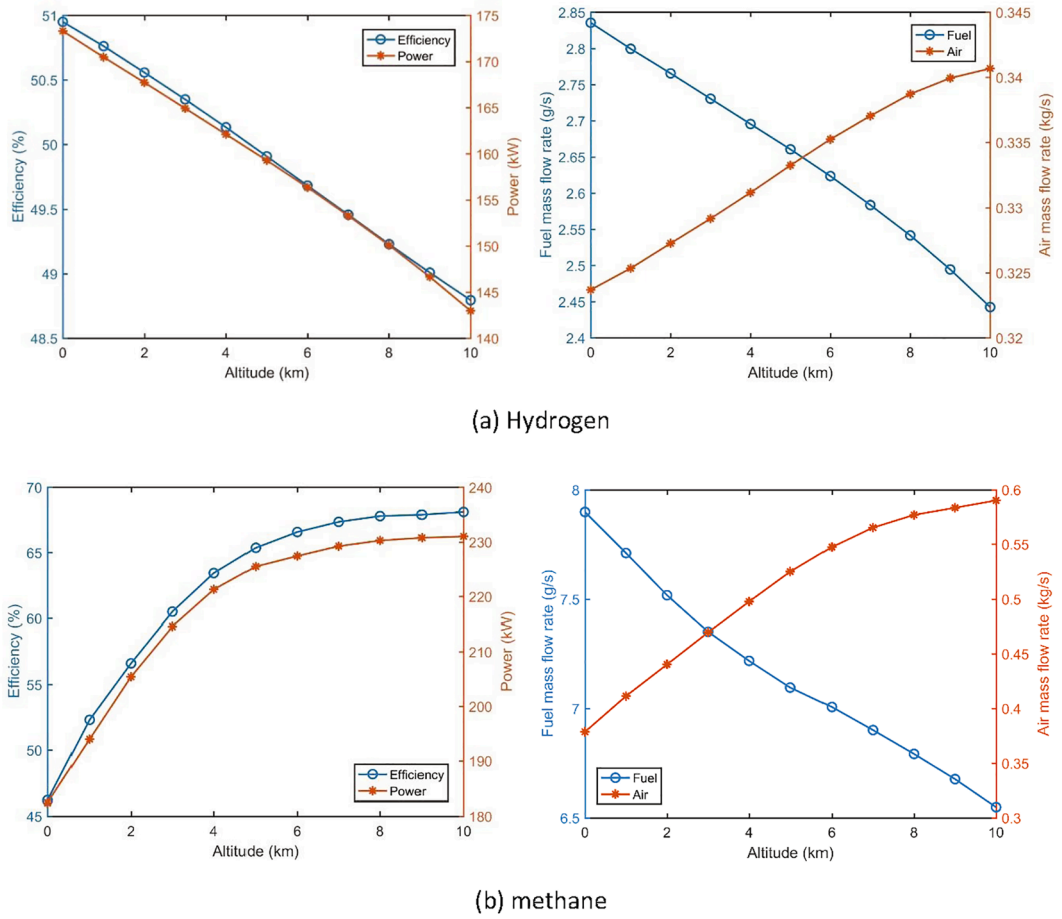

Fig. 5. System responses to changes of flight altitude.

One of the main concerns for the UAV or any other plane is the weight of the plane. In this optimization, the number of the cells will affect the weight of the UAV which changes the required thrust of the UAV. In this optimization, the thrust-to-weight ratio for the UAV is considered as a constant. We know that bigger and heavier SOFC may not necessarily be a better option since it will increase the weight and needs more fuel (for the constant thrust-to-weight ratio) which reduces the flight time. In this optimization, we have obtained the best size (cell number) to maximize the thrust and flight time while minimizing the weight and fuel consumption.

4. Validation

The results of the simulation of the proposed propulsion system have been compared to similar results reported by other authors. For this purpose, the working conditions of the proposed system by Zhixing et al [51] were used for simulating the system proposed in this study. Tables 10–12 compares the simulated temperature and pressure of the current study for each point also, efficiency and thrust with data reported by Zhixing et al [51]. As we see, a desirable agreement can be noticed.

Also, a similar comparison has been conducted for the methane-fuel system in Table 11.

Additionally, Table 12 compares efficiency, Cell voltage and thrust for proposed systems with results reported by Zhixing [51] et al.

Fig. 3 shows the result of the present study's SOFC mathematical model for calculating fuel cell's voltage and current density compared to results obtained by Chen et al. [46].

5. Results

In the case of comparing the performance of two hybrids turbine-less configurations of the supersonic propulsion system in this study, a numerical simulation of the operating condition is performed. Firstly, the weight of the UAV with regard to the SOFC size has been estimated, and due to this variable, the amount of required thrust for the vehicle can be calculated. furthermore, the performance of the two systems is compared by different parameters such as the flight altitude, fuel mass flow rate, compressor pressure ratio, and the SOFC temperature. Finally, the optimum amounts of the thrust and fuel consumption as the key parameters of the system performance are calculated by the TOPSIS method.

As we mentioned previously, by changing the weight (percentage of the impact of each goal) for the dimensionless thrust and fuel mass flow rate in the multi-objective optimization target, the optimum working condition will change. These working points create a working curve in which each point on this curve is related to a specific weight as shown in Eq. (49). This working curve which is known for the Pareto frontier is demonstrated in Fig. 4. If the weight is set to 1, optimization will only maximize the thrust with no restriction on the fuel mass flow rate (A); Subsequently, if weight is set to 0, optimization will only minimize the fuel mass flow rate with no restriction on the thrust (B).

For obtaining the best working point for these proposed systems, we used the TOPSIS decision-making method. This method designates two points as imaginary best and worst points and selects the optimum answer in a way that the selected point has the minimum and maximum distances to the imaginary best and worst points, respectively. The optimum working conditions for both proposed propulsion systems are illustrated in Table 13. Also, stream properties of the hydrogen- and

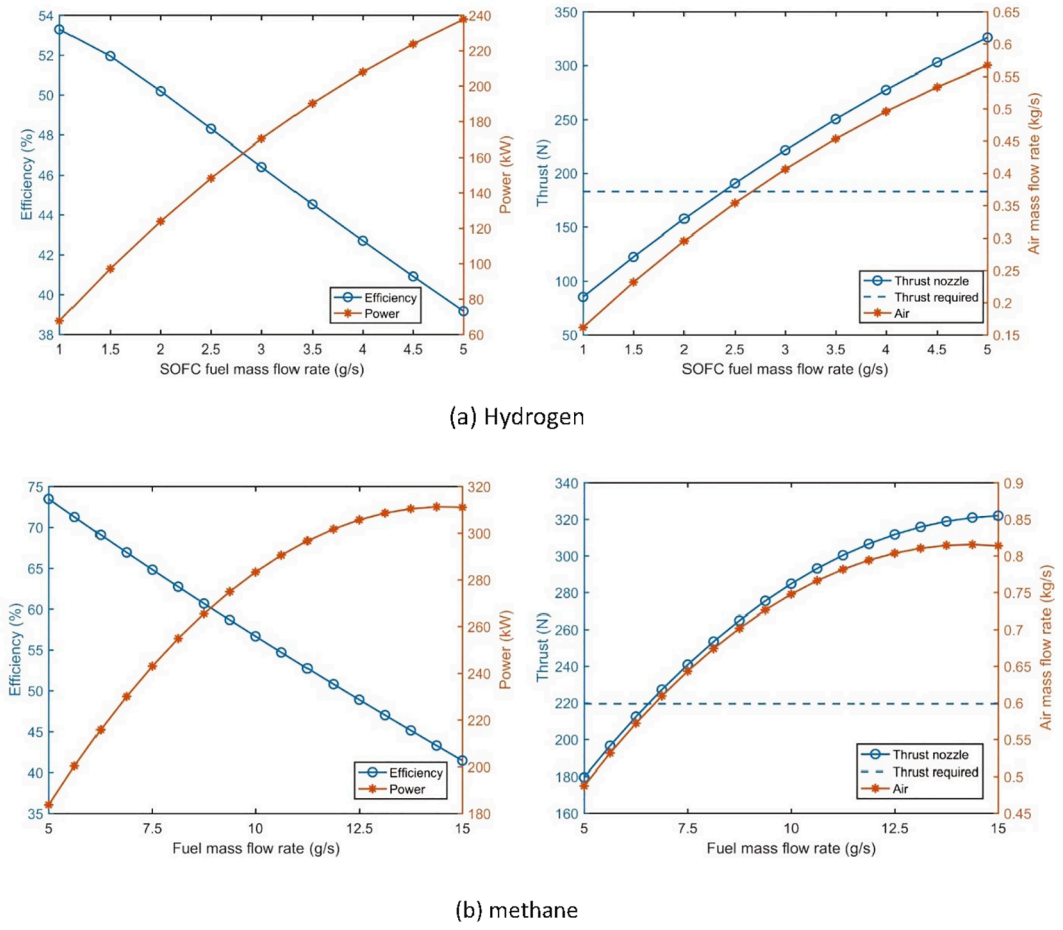

Fig. 6. System responses to changes of the SOFC's fuel mass flow rate.

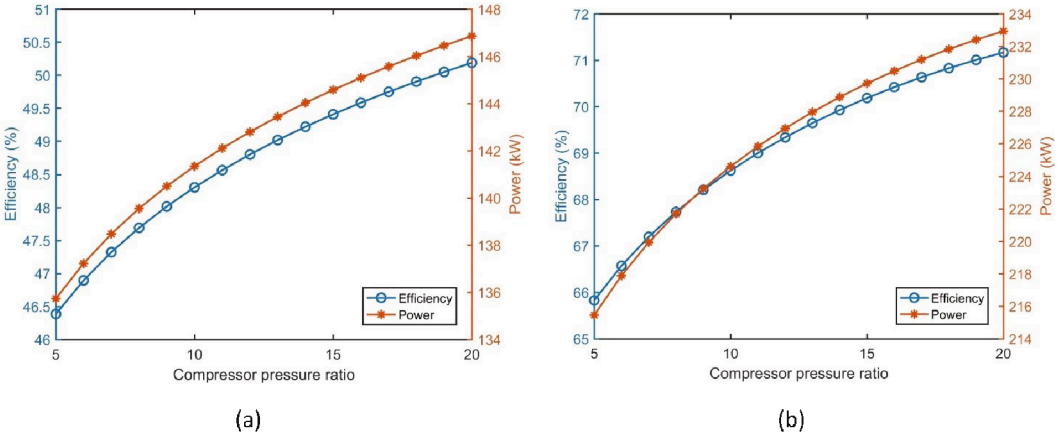

Fig. 7. Efficiency and power changes as a function of Compressor pressure ratio. a) hydrogen-fueled system. b) Methane fueled system.

methane-fueled propulsion systems are shown in Table 14 and Table 15, respectively.

For studying system responses to changes in key design parameters and different flight altitudes, we performed a sensitivity analysis to find out the changes in efficiency, SOFC's power generation, fuel, and air mass flow rate and thrust based on which parameter is investigated. For this purpose, we fix all the key design parameters at the optimum operation condition obtained from GA results and TOPSIS methods' decision and vary a single parameter in the range in which the system can be operated at. In the following, we discuss each of these key parameters.

5.1. Flight altitude

It's clear that in different altitudes the physical properties of the air (e.g. temperature, pressure, density, etc.) will change so that the system performance needs to be assessed at different flight levels. As illustrated in Fig. 5, for the methane-fueled system the efficiency and generated power of the propulsion system increases as flight altitude rises; This is due to the existence of the reformer and recirculation of unused fuel

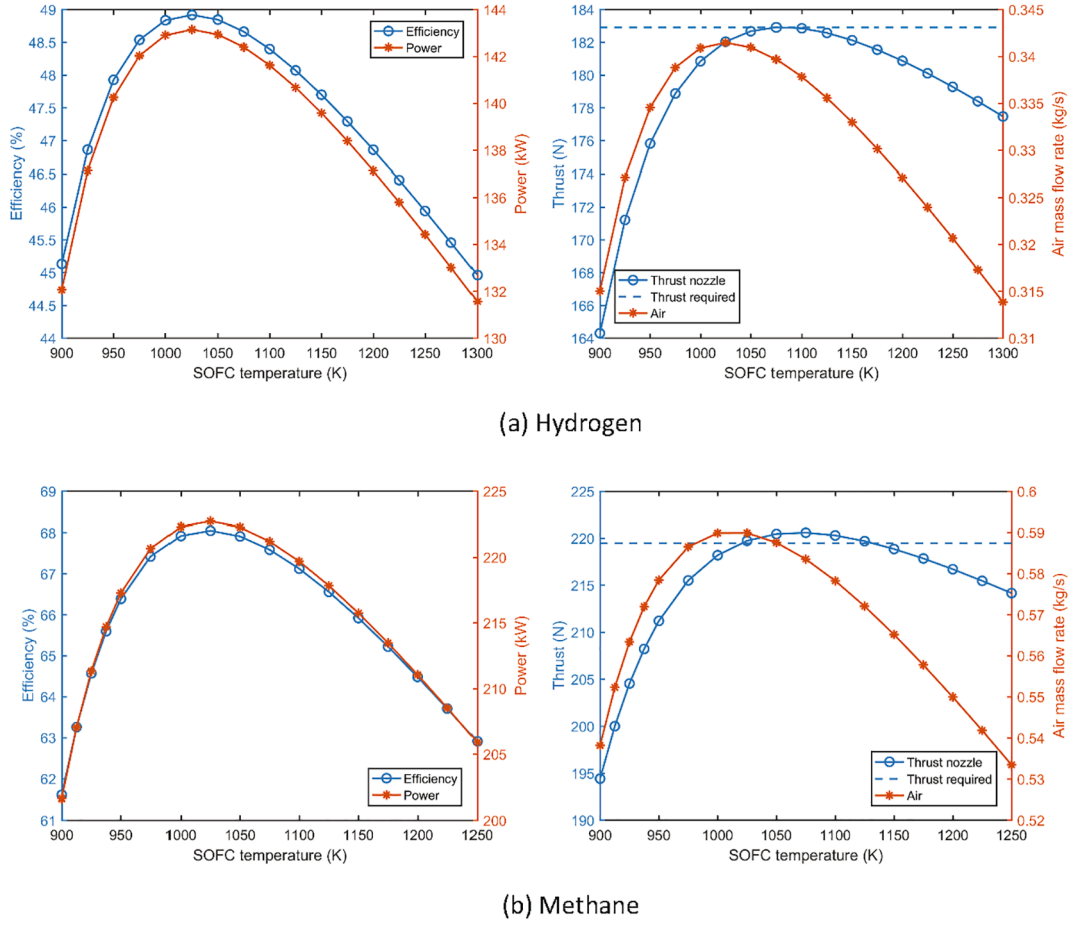

Fig. 8. System responses to changes in the stack temperature.

which affects the fuel utilization inside the SOFC thus resulting in higher thermal efficiency. This phenomenon can help the UAV to be capable of operating at high-altitude missions. On the other hand, the hydrogen-fueled system shows more potential for low-altitude missions since by increasing the altitude, the efficiency drops; Contradicting to the hydrogen-fueled system, the methane-fueled system's efficiency increases in higher altitudes and ultimately became constant which is ideal for long-term flights in high altitudes. In both systems, we can see that the fuel consumption rate will drop as altitude increases due to lower air temperature, which reduces compressor power and decreases in the air resistance force which requires lower thrust. However, the air mass flow rate increases in higher altitudes.

5.2. SOFC fuel mass flow rate

The amount of thrust which is generated by an engine is important. But the amount of fuel used to generate that thrust is sometimes has more significant importance since the UAV has to lift and carry the additional fuel with the main necessary instruments for the long-endurance missions. As depicted in Fig. 6, increasing the fuel mass flow rate of the SOFC by when other key parameters are in optimum condition will generate extra electrical power and higher thrust for the UAV; But this higher fuel rate will decrease the efficiency thus resulting in lower flight endurance. Results state that the hydrogen-fueled SOFC system is a suitable candidate for a fuel mass flow rate range of 1 to 5 g/s and a power range of 60 to 240 kW. however, the methane-fueled system exhibits a power range of 180 to 320 kW and a fuel mass flow rate of 5 to 15 g/s. Also, it should be noted that the fuel mass flow rate cannot be lower than 2.4 g/s and 6.56 g/s for hydrogen-fueled and methane-fueled systems, respectively; Since the generated thrust became insufficient for maintaining the current speed and altitude of the UAV.

5.3. Compressor pressure ratio

The pressure ratio is considered a major factor in the operation of UAVs with hybrid turbine-less SOFC jet engines. Fig. 7 demonstrates the system responses to changes in compressor pressure ratio in Mach 1.8. As we see, the efficiency of power generated by the SOFC propulsion system and thrust raise with the increase of compressor pressure ratio. This increase in the thrust for the propulsion power is due to the increment of the nozzle pressure ratio. furthermore, by increasing the pressure ratio of the compressor and constancy of the generated electric power of the fuel cell, the efficiency of the fuel cell lightly increases. By correlating Fig. 7a and 7b this is concluded that the hydrogen-fueled system generates less power and has lower efficiency and this can be due to higher utilization of fuel which with the help of recirculation of the unused fuel.

5.4. Stack temperature

As we see in Fig. 8, stack temperature plays a major role in the efficiency of the SOFC power generation which also effectively changed the thrust of the engine. As indicated in the figures, for both hydrogen- and methane-fueled systems, maximum efficiency happens around the stack temperature of 1025 K, but this is not in agreement with where the maximum thrust happens which is around 1075 K. So, it can be concluded that whether optimization target is set to maximum efficiency or thrust, operating conditions may differ which is the main reason why the cruise speed is different and lower than the maximum speed in the airplanes. Additionally, since one of the objectives of the optimization is

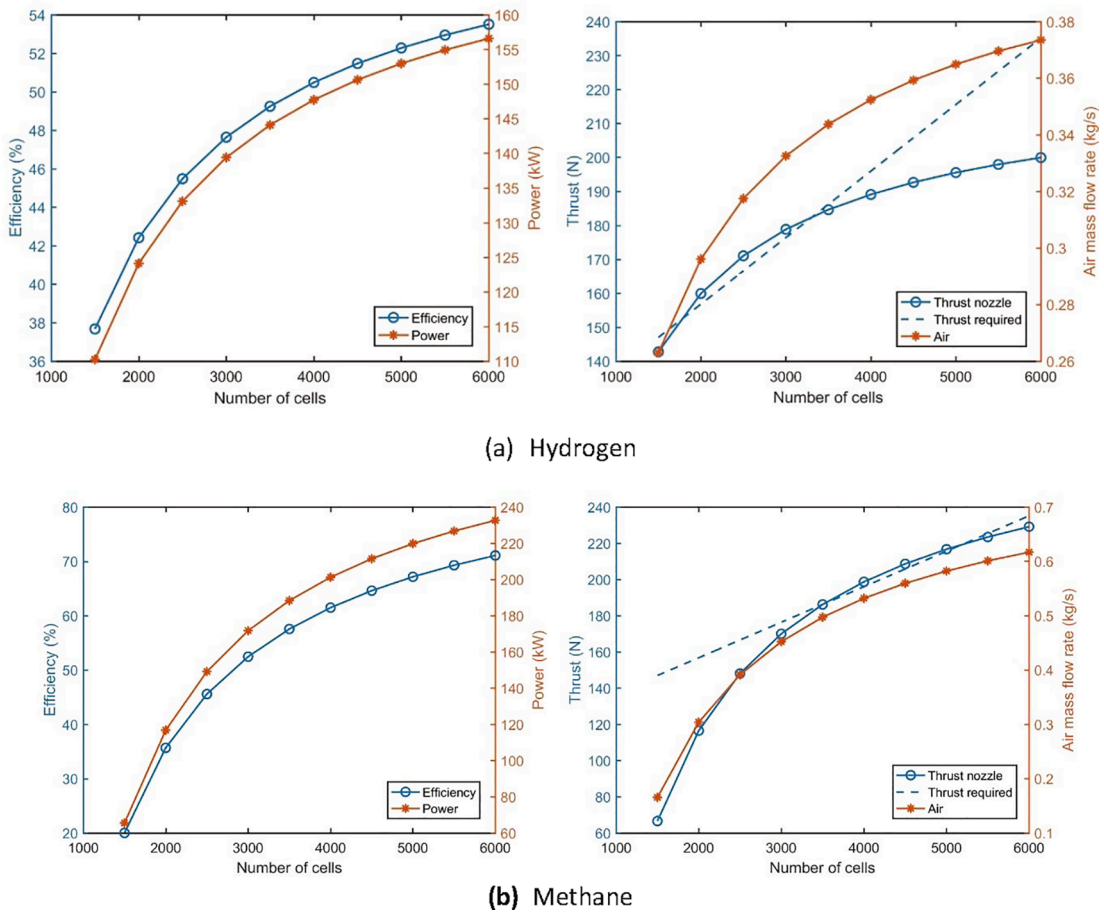

Fig. 9. System responses to changes in the number of the cells.

minimizing the fuel consumption, as we see in the figure, at the optimum working conditions, available thrust from the engine and required thrust for maintaining the current flight profile is equivalent; So even the slightest changes in the stack temperature may result in inconsistency in flight profile which is not demanding. From this fact, we suggest that future researchers that use a similar pattern for optimization or designing UAV engines, use a safety factor to ensure that this inconsistency never happens for at least small changes.

5.5. Cell numbers

Although the number of cells in the SOFC is constant and won't change during the flight and midair, however different number of cells will result in different voltage and current which varies the generated power of the SOFC as increasing the cell numbers will increase the efficiency and thrust; Moreover, changing the number of cells varies the weight of the UAV and change the required thrust and power. As we see in Fig. 9, increasing the cell numbers will result in higher power generation and thrust but as we see, if the number of cells increases without changing the other design parameters, there is a lower and upper limit for the cell number. As indicated in Fig. 9, for the hydrogen-fuel system, the range of available cell numbers is from 1750 to 3250. And for the methane-fuel system, the mentioned range is from 3500 to 5250.

6. Conclusion

In the case of comparing the performance of two hybrid turbine-less configurations of the supersonic power unit in this study with hydrogen and methane as different types of fuel, a numerical simulation of the operating condition is performed. The thermodynamic parameters of both systems are studied under the condition of supersonic flight mode with the Mach number equal to 1.8. Finally, the generated thrust and consumed fuel as the key parameters of the flight were optimized by the Genetic algorithm and TOPSIS method. The main results of this study are shown as follow:

1. The efficiency and generated power of the propulsion system by increasing flight altitude increase in the case of the methane-fuel system.
2. Low temperature at high altitude flight levels in case of fixed Mach number and compressors pressure ratio leads to increment in intake air mass flow rate of the system.
3. The increasing fuel rate of the SOFC power unit helps the process of generating extra power and thrust for UAVs. But it should be noted that high fuel mass flow rate drops the fuel cell efficiency which generally makes the flight endurance low.
4. By increasing the pressure ratio of the compressor and constancy of the generated electric power of the fuel cell, the efficiency of the fuel cell lightly increases. the methane-fueled system generates higher power and efficiency due to the recirculation of the unused fuel.
5. By increasing the cell numbers, the efficiency of the system rises due to the improvement of the generated power and thrust. And the simulation results state that the thrust and consumed air of the hydrogen-fueled power unit are less than the methane-fueled.
6. Maximum efficiency for both hydrogen- and methane-fueled systems are available with the stack temperature of 1025 K; However maximum thrust for these systems is at the stack temperature of 1075 K.
7. For the current study, the thrust and fuel consumption were parameters that were optimized by the multi-objective optimization

method for both systems. The efficiency and fuel consumption for the hydrogen-fueled system are equal to 48.7% and 0.0024 kg/s and for the methane-fueled system are 67.9% and 0.0066 kg/s.

Declaration of Competing Interest

The authors declare that they have no known competing financial interests or personal relationships that could have appeared to influence the work reported in this paper.

References

[1] Stambouli AB, Traversa E. Solid oxide fuel cells (SOFCs): a review of an environmentally clean and efficient source of energy. Renew Sustain Energy Rev 2002;6(5):433–55.
[2] Zhang X, Chan SH, Li G, Ho HK, Li J, Feng Z. A review of integration strategies for solid oxide fuel cells. J Power Sources 2010;195(3):685–702.
[3] Buonomano A, Calise F, d'Accadia MD, Palombo A, Vicidomini M. Hybrid solid oxide fuel cells–gas turbine systems for combined heat and power: a review. Appl Energy 2015;156:32–85.
[4] Bae Y, Lee S, Yoon KJ, Lee J-H, Hong J. Three-dimensional dynamic modeling and transport analysis of solid oxide fuel cells under electrical load change. Energy Convers Manag 2018;165:405–18.
[5] Marchant W, Tosunoglu S. Rethinking wildfire suppression with swarm robotics. Proc. 29th Florida Conf. Recent Adv. Robot. FCRAR, vol. 16, 2016.
[6] Rechberger J, Kaupert A, Hagerskans J, Blum L. Demonstration of the first European SOFC APU on a heavy duty truck. Transp Res Procedia 2016;14:3676–85.
[7] Kaya N, Turan Ö, Karakoç TH, Midilli A. Parametric study of exergetic sustainability performances of a high altitude long endurance unmanned air vehicle using hydrogen fuel. Int J Hydrogen Energy 2016;41:8323–36.
[8] Cirigliano D, Frisch AM, Liu F, Sirignano WA. Diesel, spark-ignition, and turboprop engines for long-duration unmanned air flights. J Propuls Power 2018;34(4):878–92.
[9] Entezari A, Bahari M, Aslani A, Ghahremani S, Pourfayaz F. Systematic analysis and multi-objective optimization of integrated power generation cycle for a thermal power plant using Genetic algorithm. Energy Convers Manag 2021;241:114309.
[10] Papathakis K, Schnarr O, Lavelle T, Borer N, Stoia T, Atreya S. Integration Concept for a Hybrid-Electric Solid-Oxide Fuel Cell Power System into the X-57 2018.
[11] Eisavi B, Chitsaz A, Hosseinpour J, Ranjbar F. Thermo-environmental and economic comparison of three different arrangements of solid oxide fuel cell-gas turbine (SOFC-GT) hybrid systems. Energy Convers Manag 2018;168:343–56.
[12] Tucker MC. Development of High Power Density Metal-Supported Solid Oxide Fuel Cells. Energy Technol 2017;5(12):2175–81.
[13] Giacoppo G, Barbera O, Briguglio N, Cipitì F, Ferraro M, Brunaccini G, et al. Thermal study of a SOFC system integration in a fuselage of a hybrid electric mini UAV. Int J Hydrogen Energy 2017;42(46):28022–33.
[14] Azizi MA, Brouwer J. Progress in solid oxide fuel cell-gas turbine hybrid power systems: System design and analysis, transient operation, controls and optimization. Appl Energy 2018;215:237–89.
[15] Aguiar P, Brett D, Brandon N. Solid oxide fuel cell/gas turbine hybrid system analysis for high-altitude long-endurance unmanned aerial vehicles. Int J Hydrogen Energy 2008;33(23):7214–23.
[16] Waters DF, Cadou CP. Engine-integrated solid oxide fuel cells for efficient electrical power generation on aircraft. J Power Sources 2015;284:588–605.
[17] Himansu A, Freeh JE, Steffen Jr CJ, Tornabene RT, Wang X-YJ. Hybrid solid oxide fuel cell/gas turbine system design for high altitude long endurance aerospace missions 2006.
[18] Okai K, Fujiwara H, Nomura H, Tagashira T, Yanagi R. Performance Analysis of a Fuel Cell Hybrid Aviation Propulsion System. 10th Int. Energy Convers. Eng Conf 2012:4238.
[19] Okai K, Himeno T, Watanabe T, Nomura H, Tagashira T. Investigation of FC/GT hybrid core in electrical propulsion for fan aircraft. 51st AIAA/SAE/ASEE Jt Propuls Conf 2015:3888.
[20] Okai K, Nomura H, Tagashira T, Nishizawa A. Effects of Fuel Type on Aircraft Electric Propulsion with SOFC/GT Hybrid Core. 53rd AIAA/SAE/ASEE Jt Propuls Conf 2017:4957.
[21] Collins JM, McLarty D. All-electric commercial aviation with solid oxide fuel cell-gas turbine-battery hybrids. Appl Energy 2020;265:114787. https://doi.org/10.1016/j.apenergy.2020.114787.
[22] Fernandes A, Woudstra T, Aravind PV. System simulation and exergy analysis on the use of biomass-derived liquid-hydrogen for SOFC/GT powered aircraft. Int J Hydrogen Energy 2015;40(13):4683–97.
[23] Pan ZF, An L, Wen CY. Recent advances in fuel cells based propulsion systems for unmanned aerial vehicles. Appl Energy 2019;240:473–85.
[24] Yanovskiy LS, Baykov AV, Raznoschikov VV, Averkov IS. Alternative fuels and perspectives solid oxide fuel cells usage in air transport. ECS Trans 2013;57(1):149–60.
[25] Seyam S, Dincer I, Agelin-Chaab M. Novel hybrid aircraft propulsion systems using hydrogen, methane, methanol, ethanol and dimethyl ether as alternative fuels. Energy Convers Manag 2021;238:114172. https://doi.org/10.1016/j.enconman.2021.114172.
[26] Seyam S, Dincer I, Agelin-Chaab M. Exergetic assessment of a newly designed solid oxide fuel cell-based system combined with a propulsion engine. Energy 2022;239:122314. https://doi.org/10.1016/j.energy.2021.122314.
[27] Choudhury A, Chandra H, Arora A. Application of solid oxide fuel cell technology for power generation—A review. Renew Sustain Energy Rev 2013;20:430–42.
[28] Bao C, Wang Y, Feng D, Jiang Z, Zhang X. Macroscopic modeling of solid oxide fuel cell (SOFC) and model-based control of SOFC and gas turbine hybrid system. Prog Energy Combust Sci 2018;66:83–140.
[29] Stiller C. Design, operation and control modelling of SOFC/GT hybrid systems. Fakultet for ingeniørvitenskap og teknologi. 2006.
[30] Mahmoudi SMS, Khani L. Thermodynamic and exergoeconomic assessments of a new solid oxide fuel cell-gas turbine cogeneration system. Energy Convers Manag 2016;123:324–37.
[31] Lv X, Lu C, Wang Y, Weng Y. Effect of operating parameters on a hybrid system of intermediate-temperature solid oxide fuel cell and gas turbine. Energy 2015;91:10–9.
[32] Lv X, Gu C, Liu X, Weng Y. Effect of gasified biomass fuel on load characteristics of an intermediate-temperature solid oxide fuel cell and gas turbine hybrid system. Int J Hydrogen Energy 2016;41(22):9563–76.
[33] Lv X, Lu C, Zhu X, Weng Y. Safety analysis of a solid oxide fuel cell/gas turbine hybrid system fueled with gasified biomass. J Fuel Cell Sci Technol 2015;12.
[34] Ji Z, Qin J, Cheng K, Guo F, Zhang S, Zhou C, et al. Determination of the safe operation zone for a turbine-less and solid oxide fuel cell hybrid electric jet engine on unmanned aerial vehicles. Energy 2020;202:117532. https://doi.org/10.1016/j.energy.2020.117532.
[35] Lv X, Liu X, Gu C, Weng Y. Determination of safe operation zone for an intermediate-temperature solid oxide fuel cell and gas turbine hybrid system. Energy 2016;99:91–102.
[36] Jansen R, Brown GV, Felder JL, Duffy KP. Turboelectric aircraft drive key performance parameters and functional requirements. 51st AIAA/SAE/ASEE Jt Propuls Conf 2015:3890.
[37] Roth B, Giffin R. Fuel cell hybrid propulsion challenges and opportunities for commercial aviation. 46th AIAA/ASME/SAE/ASEE Jt Propuls Conf Exhib 2010:6537.
[38] Ly LT. Computational Investigation and Experimental Validation of a Small Subsonic Turbine-less Jet Engine Concept. Los Angeles: California State University; 2010.
[39] Eiguren T, Douglas T, Buchanan T. Unmanned Aerial Vehicle (UAV) Propulsion Research: Conceptual Studies of "Ultra-Compact Shaft-Less. Jet Engines" for Next Generation UAVs 2015.
[40] Buchanan T, Anderson I, Woodard S. Ultralight Turbine-less Jet Engine 2016.
[41] Ji Z, Rokni MM, Qin J, Zhang S, Dong P. Performance and size optimization of the turbine-less engine integrated solid oxide fuel cells on unmanned aerial vehicles with long endurance. Appl Energy 2021;299:117301. https://doi.org/10.1016/j.apenergy.2021.117301.
[42] Ji Z, Qin J, Cheng K, Liu H, Zhang S, Dong P. Thermodynamic analysis of a solid oxide fuel cell jet hybrid engine for long-endurance unmanned air vehicles. Energy Convers Manag 2019;183:50–64.
[43] Martinez AS, Brouwer J, Samuelsen GS. Comparative analysis of SOFC–GT freight locomotive fueled by natural gas and diesel with onboard reformation. Appl Energy 2015;148:421–38.
[44] Pirkandi J, Ghassemi M, Hamedi MH, Mohammadi R. Electrochemical and thermodynamic modeling of a CHP system using tubular solid oxide fuel cell (SOFC-CHP). J Clean Prod 2012;29:151–62.
[45] Pirkandi J, Mahmoodi M, Ommian M. An optimal configuration for a solid oxide fuel cell-gas turbine (SOFC-GT) hybrid system based on thermo-economic modelling. J Clean Prod 2017;144:375–86.
[46] Chan SH, Khor KA, Xia ZT. A complete polarization model of a solid oxide fuel cell and its sensitivity to the change of cell component thickness. J Power Sources 2001;93(1-2):130–40.
[47] Aguiar P, Adjiman CS, Brandon NP. Anode-supported intermediate temperature direct internal reforming solid oxide fuel cell. I: model-based steady-state performance. J Power Sources 2004;138(1-2):120–36.
[48] Korakianitis T, Wilson DG. Models for predicting the performance of Brayton-cycle engines. Turbo Expo Power Land, Sea, Air, vol. 78941, 1992, p. V002T02A020.
[49] Entezari A, Manizadeh A, Ahmadi R. Energetical, exergetical and economical optimization analysis of combined power generation system of gas turbine and Stirling engine. Energy Convers Manag 2018;159:189–203. https://doi.org/10.1016/j.enconman.2018.01.012.
[50] Bahari M, Ahmadi A, Dashti R. Exergo-economic analysis and optimization of a combined solar collector with steam and Organic Rankine Cycle using particle swarm optimization (PSO) algorithm. Clean Eng Technol 2021;4:100221. https://doi.org/10.1016/j.clet.2021.100221.
[51] Ji Z, Qin J, Cheng K, Guo F, Zhang S, Dong P. Comparative performance analysis of solid oxide fuel cell turbine-less jet engines for electric propulsion airplanes: Application of alternative fuel. Aerosp Sci Technol 2019;93:105286.